Vibronic structure in the "metallic" reflection band of the $TCNQ^0$ crystal[a)]

M. R. Philpott, P. M. Grant, K. Syassen,[b)] and J-M. Turlet[c)]

IBM Research Laboratory, San Jose, California 95193
(Received 5 May 1977)

Polarized reflection spectra off the (010) face of the first singlet transition of crystalline tetracyanoquinodimethane ($TCNQ^0$) have been measured at room and liquid helium temperatures. The spectrum consists of a massive block of high reflectivity, corresponding to a stop band 1.4 eV wide, with well defined edges at 2.8 and 4.2 eV. The reflectivity of the long wavelength edge undergoes a large increase upon cooling, and vibrational structure appears between 2.8 and 3.1 eV due to freezing out of powerful polariton scatterers, the intramolecular vibrations. All structure is assoicated with volume polaritons since it is not shifted when the crystal is coated with a layer of frozen gas. The complex dielectric function, calculated by a Kramers–Kronig transformation, shows two regions where the real part ϵ_1 is negative. The spectra provide a test of the basic notions of strong vibronic coupling in molecular crystals. Polariton scattering by lattice phonons is weak, wherea scattering by intramolecular modes is much stronger.

I. INTRODUCTION

Exciton bands of great width occur in organic solids when the oscillator strength of the molecular transition is greater than unity. Some exciton bands have widths comparable to the molecular excitation energy. Crystal faces upon which the transition moment has a large projection display high reflectivity over intervals spanning several electron volts. Within these regions the reflectivity may get as high as 80% to 90%, and the crystal faces assume a distinct metallic appearance. This phenomenon is referred to as *metallic reflection from organic solids*.

Until recently, the best characterized example of metallic reflection was that due to the 280 nm transition of anthracene[1–5] (oscillator strength $f = 1.6$). However, metallic reflection from anthracene is a difficult one to study experimentally because of its location in the uv. From the theoretical viewpoint there are complications due to overlap with several electronic transitions of ill defined parentage and the presence of lower lying singlet transitions to which relaxation is rapid. Recently, Pennelly and Eckhardt[6] found that at room temperature the (010) face of 7, 7', 8, 8'-tetracyanoquinodimethane ($TCNQ^0$) had a blue metallic reflection band of the same general shape as found in the classic case of 1, 5-*bis*-(dimethylamino)pentamethinium perchlorate[7–8] (BDP), only with more vibronic structure. The attributes of $TCNQ^0$ that make it attractive for further experimental and theoretical study are its spectrum in the visible, high symmetry (D_{2h}) and well defined crystal structure[9] ($C2/c$ with four molecules per unit cell). In passing, we note the interesting observations by Hesse, Fuhs, and Weisser of *silver* metallic reflection from the (110) face of γ-cyclopropyl-*bis*(1, 3, 3-trimethylindolenin-2-yl) pentamethinium tetrafluoroborate crystals.[10] Metallic reflection in this cationic dye starts at 1.75 eV and spans most of the visible.

In this paper we report the polarized reflection spectra of the first singlet transition ($^1B_{3u} \leftarrow {}^1A_{1g}$, oscillator strength $f = 0.94$, see Ref. 6) of $TCNQ^0$ crystals off the (010) face at liquid helium temperatures. This work was undertaken with the aim of obtaining data to test the so-called strong vibronic coupling theory of excitons in organic materials.[11,12] All room temperature reflection spectra show only broad maxima and therefore provide no insight regarding the coupling of particular vibrational modes to the electronic excitation.

II. EXPERIMENT

Low temperature reflection spectra were taken off an uncleaved natural (010) face of a crystal grown by slow cooling of a saturated solution of $TCNQ^0$ in acetonitrile. Spectra were also taken off (010) faces obtained by cleaving large solution grown crystals. The reflection minima and maxima did not vary in energy, though there were differences in intensity due to differences in surface roughness. Figure 1 shows a detail of the low energy reflection edge taken at 6 K with a cleaved crystal immersed in He gas, and the resolution is 1 Å ($\simeq 6$ cm^{-1}). Cooling to 2 K had no further effect. Figures 2–4 show the 13 K reflection spectrum and the derived optical constants of a natural (010) face. Reflection data gathered at 13 K were taken at 5 Å ($\simeq 30$ cm^{-1}) intervals in regions with the fine structure. In all spectra the incident light was polarized with the electric vector parallel to the direction of maximum reflectivity. The angle of incidence in the spectra of Figs. 2–4 was 18° and the incident beam was focussed into a cone with an angle of 10°. The spectrum in Fig. 1 was taken using light focussed onto the crystal using a ×15 Beck reflecting objective. In this latter arrangement the cone angle was approximately 25°, with the axis of the objective perpendicular to the crystal face, so that the angle of incidence was less than 13°.

The difference between the room temperature and low

[a)] A preliminary account of this work was given at the March meeting of the American Physical Society, Denver, Colorado, 1975. See J-M. Turlet, P. M. Grant, and M. R. Philpott, Bull. Am. Phys. Soc. 20, 414 (1975).

[b)] IBM World Trade Postdoctoral Fellow 1976–77.

[c)] IBM World Trade Postdoctoral Fellow 1974–75. Present address: Laboratoire d'Optique Moléculaire, Université Bordeaux I, Talence 33405, France.

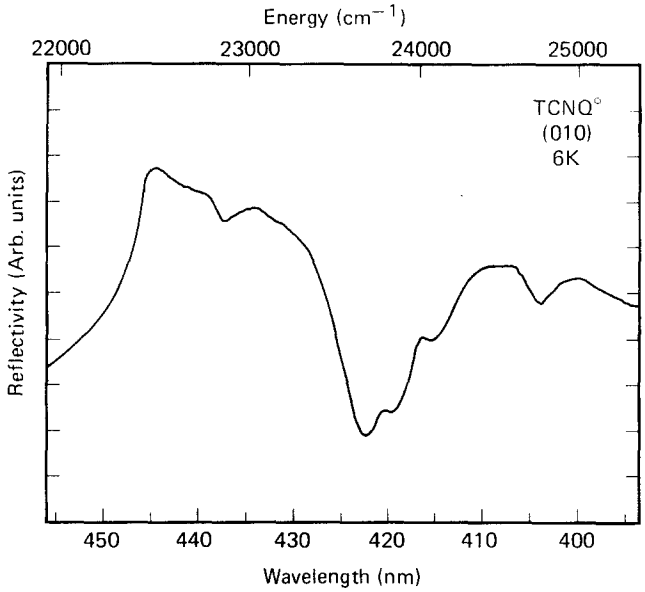

FIG. 1. Reflection spectrum of a freshly cleaved $TCNQ^0$ crystal off the (010) face for $E \parallel R_{max}$ at 6 K.

temperature spectrum consisted of a substantial increase in the reflection power of the low energy edge, a concomitant decrease in reflectivity in the deep minimum near 423 nm, and the appearance of subsidiary maxima and minima throughout the region from 444 to 385 nm. Fine details of this type have never been observed in metallic reflection from an organic solid. We do not think that this effect is unusual; quite the reverse, we expect all strong transitions to show vibrational details similar to those reported here, provided the exciton transition lies at or close to the bottom of the exciton band and the molecule has high symmetry such as D_{2h}. Transitions at or near the bottom of the band are the ones least affected by relaxation or scattering processes since the density of excited states is low. High symmetry will in general greatly restrict the number of intramolecular modes participating in the electronic transition thereby keeping spectral congestion to a minimum.

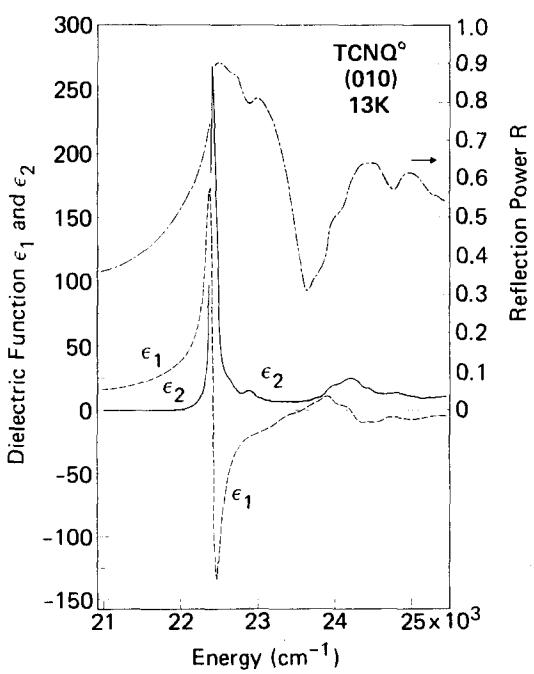

FIG. 2. Complex dielectric function ϵ_1 and ϵ_2 obtained by Kramers-Kronig transformation of the (010) reflection spectrum. Data taken at 13 K using a crystal grown from solution. ---ϵ_1, —ϵ_2, -·-·-R.

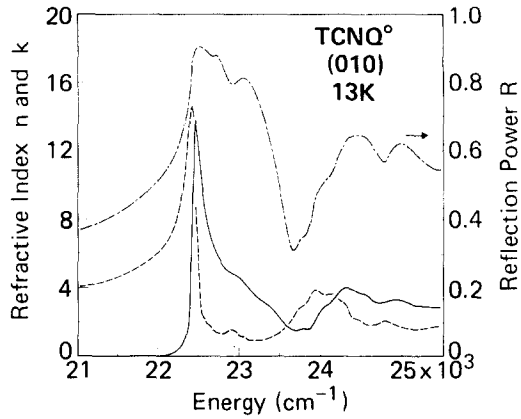

FIG. 3. Complex refractive index n and k obtained by Kramers-Kronig transformation of the (010) reflection spectrum. Data taken at 13 K using a crystal grown from solution. ---n, —k, -·-·R.

III. RESULTS AND DISCUSSION

The $TCNQ^0$ crystal at room temperature has space group $C2/c$ and the unit cell (dimensions $a = 8.906$ Å, $b = 7.060$ Å, $c = 16.395$ Å, $\beta = 98.54°$) contains four molecules. The crystal may be viewed as a stack of (001) planes in which the molecules lie in chains parallel to [110]. Within each plane all molecules are translationally equivalent if we include fractional translations $\frac{1}{2}(\mathbf{a}+\mathbf{b})$. Molecules on adjacent planes are related by the twofold screw rotation or the glide plane.

If all the transition intensity is concentrated in a single level (purely electronic excitation model), the exciton band has four branches, one for each molecule in the unit cell. In any (001) plane the molecules at 0 and $\frac{1}{2}(\mathbf{a}+\mathbf{b})$ are parallel, and consequently there are only two allowed $\kappa = q_{photon}$ transitions out of a possible four. One of these

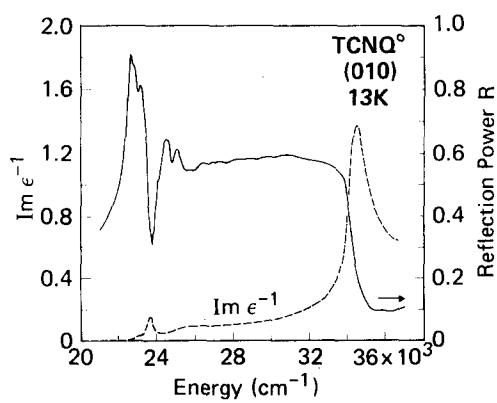

FIG. 4. Imaginary part ϵ^{-1} calculated with the complex dielectric function of Fig. 2. Reflection data taken at 13 K using a crystal grown from solution. ---Imϵ^{-1}, —R.

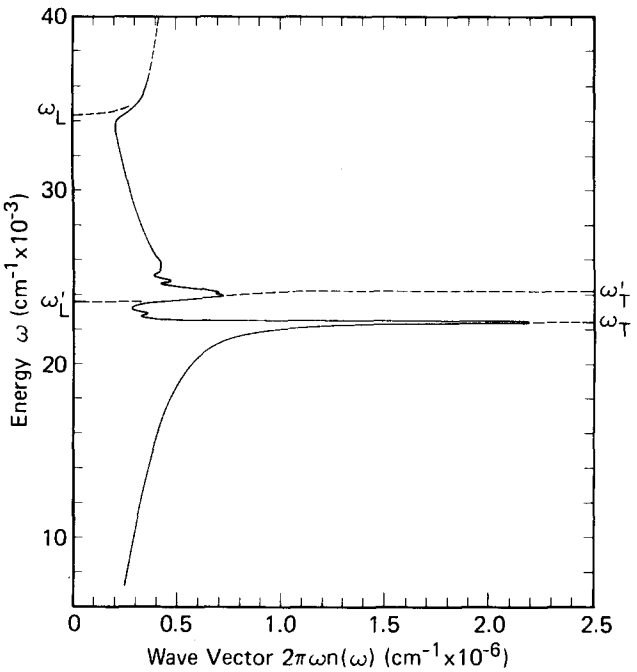

FIG. 5. Dispersion of the polariton (solid line) calculated from the reflectivity data by plotting the energy $\omega(cm^{-1}$; $\omega = E/hc)$ of the polariton versus the wave vector $\kappa = 2\pi\omega n(\omega)$, where $n(\omega)$ is the real part of the refractive index. The dispersion of the model three branch polariton is shown schematically by the broken lines only where it differs from the real polariton.

is polarized parallel to the b crystallographic axis and the other is polarized perpendicular to it in the (010) or ac plane. In the configuration of our experiment the b transition is not observed, and the ac exciton transition being transversely polarized does not have a macroscopic electric field. The ac transition is very intense since the L (long) axis of the molecule only makes an angle of approximately 25° with the (010) plane.

A. Kramers-Kronig analysis

The complex refractive index and dielectric function were calculated by Kramers-Kronig transformation of the reflectivity measured at 13 K off the (010) face. Results for selected spectral regions are shown in Figs. 2–4. The transformation was pinned by assuming the reflectivity at 20 000 cm^{-1} was due to a real refractive index $n(\omega)$. On the high frequency side the reflectivity was assumed to fall off according to a simple power law. The main sources of error are most likely the assumption of normal incidence and plane polarization implied in the use of the Fresnel equation

$$R(\omega) = \left|[\tilde{n}(\omega) - 1]/[\tilde{n}(\omega) + 1]\right|^2 .$$

In the Fresnel model the solid is treated as a continuum with complex refractive index $\tilde{n}(\omega)$. There is no explicit correction for reconstructed planes at the crystal surface. Likewise, spatial dispersion of the dielectric function and frequency dispersion of the dielectric axis are ignored. The latter effect can be neglected for $TCNQ^0$ because of the intensity of the molecular transition and the absence of any close transitions of different polarization.

The derived spectra for ϵ_1, ϵ_2, $\mathrm{Im}\epsilon^{-1}$, and the real (n) and imaginary (k) parts of $\tilde{n}$ allow one to determine parameters useful for the interpretation of the reflection spectrum. In a model in which all vibrational structure is ignored, and the transitions assumed to have all intensity concentrated in a single level (pure electronic excitation model), the width of the stop band[13] is determined by the difference in the energies of a transverse and longitudinal exciton. Peaks in ϵ_2 and $\mathrm{Im}\epsilon^{-1}$ locate transverse and longitudinal excitations, respectively. From Figs. 2 and 4 we see that the lowest transverse exciton is at $\omega_T = 22\,420$ cm^{-1} and the highest longitudinal exciton has $\omega_L = 34\,350$ cm^{-1}. The width of the stop band is therefore 11 900 cm^{-1}. The second most intense peak in ϵ_2 occurs at $\omega'_T = 24\,180$ cm^{-1}. There is also a second longitudinal mode prominent in Fig. 4 at $\omega'_L = 23\,580$ cm^{-1}, close to the minimum in reflection at 23 650 cm^{-1}. The two major and two minor exciton oscillators suggest an approximate empirical model for the optical characteristics of the (010) face. In this model the reflection spectrum is decomposed into the stop bands of a three branch polariton. Figure 5 shows *schematically* the dispersion of this three branch model (broken lines) superimposed on the experimentally determined polariton dispersion (solid line). The latter was calculated from the reflectivity data by plotting $\omega(cm^{-1}$; $\omega = E/hc)$ versus the wave vector $\kappa = 2\pi\omega n(\omega)$, where $n(\omega)$ is the real part of the refractive index displayed in Fig. 3. We show only those portions of the three branch polariton curve that differ from the experimental one. The lower or first branch has a cutoff at ω_T, the middle or second runs between ω'_L and ω'_T, and the upper or third branch starts at ω_L and curves towards the light line. This empirical model is nothing more than a convenient way of characterizing the response of the crystal to the incident light. Although it presently provides no insight into exciton–phonon processes occurring within the crystal, it does hint at some correlations between peaks in the reflection spectrum that are pointed out in Sec. III. C. However, before turning to this subject we touch upon two other topics of interest.

B. Surface excitons and surface polaritons

The presence of deep reflection minima within reflection bands may be due to surface transitions or according to strong vibronic coupling theory to two-particle and higher multiparticle transitions. In anthracene there are surface transitions within the stop band of the first singlet transition at 400 nm which give rise to deep reflection minima.[14] To test for the presence of surface transitions in the (010) spectra the crystal was exposed to air while maintained at a low temperature (≃ 20 K). No shifts in maxima or minima of the type observed in the anthracene spectra were observed. We conclude therefore that all features in the (010) spectra recorded in the experiments described here were due to bulk transitions.

In Fig. 2 it is evident that $\epsilon_1 < -1$ and $|\epsilon_1| \gtrsim 2\epsilon_2$ between $\omega = 22\,520$ and 23 100 cm^{-1}. This region spans most of the region of intense reflectivity but not the region of the reflection minimum. The existence of $\epsilon_1 < -1$ is a necessary condition for the occurrence of surface

polaritons. Preliminary calculations using a uniaxial model suggest their existence on the (010) face of $TCNQ^0$ when excited by an ATR experiment with the plane of incidence being normal to (010) and parallel to the direction of the maximum in reflection power R.

C. Vibronic structure

There are two ways of analyzing the structure in the reflection spectrum. The first uses the phenomenological model introduced in Sec. III.A, whereas the second more physical way is based on the concept of the dressed polariton.

At the end of Sec. III.A we briefly described a phenomenological model in which the reflection band was ascribed to two stop bands (see Fig. 5). Separating the two was a branch to the polariton spectrum starting at ω_L' and ending at ω_T'. It is of some interest to determine the penetration depths, given by $d=\lambda/(4\pi k)$, where k is the imaginary part of the complex refractive index shown in Fig. 3. At frequencies ω_T, ω_L', and ω_T' the penetration depths are 25, 190, and 90 Å, respectively. These latter numbers are so small that the middle branch of the polariton in the empirical model cannot be regarded as propagating in the bulk. In spite of this difficulty the phenomenological model does have uses. For example, if the second largest peak in ϵ_2 at 24 180 cm^{-1} is assigned to a second phenomenological transverse exciton transition, then a duplication of the reflection between 450 and 425 nm is expected. The region between 415 and 390 nm contains hints of this. The peak at 408 nm is broad, suggesting the presence of a shoulder analogous to the one at 441 nm, and it is followed by a distinct minimum at 404 nm and maximum at 400 nm. An exact duplication is not expected since the peak at ω_T' is broad, and throughout this region the underlying density of electronic and vibrational states is much more complicated than in the region 450 to 425 nm where there are no high frequency C–C stretching modes.

In the strong vibronic coupling limit the width of the purely electronic band is much greater than the energy spanned by the absorption spectrum of the free molecule. In the extreme limit the exciton propagates so rapidly that no nuclear relaxation occurs around the exciton and the absorption spectrum becomes a delta function. This limit may also be described as weak exciton–phonon coupling. To avoid confusion between these terminologies we will adhere to the former and refer to the case under discussion as strong vibronic coupling.

The dressed polariton (or exciton) picture provides the simplest model in the strong coupling regime. The polariton is accompanied by a cloud of lattice phonons and molecular vibrations. This cloud may have single-particle and multiparticle components, i.e., it may consist of states corresponding to a propagating vibronic exciton (electronic and vibrational excitations occupying the same site) and also states where the electronic and vibrational excitations occupy separate sites. For wave vectors κ where the exciton–photon mixing is strong it is more accurate to describe the single-particle state as a polariton and the two-particle states as a polariton plus an intramolecular phonon. The cloud dressing of the polariton depends on ω and κ. The lowest energy excitons will have a virtual cloud since they will lie below the threshold for phonon emission. As ω is increased thresholds will be passed corresponding to the emission of lattice phonons and vibrational excitons. If we neglect coupling to acoustic phonons then the low energy part of the band will consist of a region of a single-particle states (see Ref. 15 for more details) and the reflection power of the crystal should be unity. This explains why the reflectivity of the (010) face is so high on the low energy side of the metallic reflection band.

As ω increases the reflectivity should drop rapidly as multiparticle thresholds are successively reached and passed. This decrease in reflectivity is not monotonic since it will also be determined by the density-of-states and Franck–Condon factors. Eventually, the reflectivity will rise as ω approaches the longitudinal exciton frequency ω_L because of reduced coupling brought about by the combination of vanishing Franck–Condon factors and large energy separation from the allowed transition at ω_T. The latter make the creation of multiparticle states by photon absorption highly improbable. The main minimum in reflection at 423 nm is not caused by strong crystal absorption at this wavelength. It comes about because ϵ_1 crosses the ω axis and becomes positive until $\lambda = 414$ nm is reached where it dips below the axis again. This behavior is somewhat reminiscent of the reflectivity of Ag where interband transitions depress the Drude edge to 4 eV.[16] In the case of $TCNQ^0$ the transitions causing the reflectivity to dip are centered around 412 nm (near $\omega_T' = 24\,180$ cm^{-1}). The longitudinal exciton at $\omega_L' = 23\,580$ cm^{-1} almost coincides with the main reflection mimimum.

According to the discussion presented above the complex dielectric function should have the form

$$\epsilon(\omega) = \epsilon_0 + \frac{\omega_p^2 f}{\Omega_T^2(\omega) - \omega^2} \tag{1}$$

provided spatial dispersion is negligible. Here

$$\Omega_T(\omega) = \omega_1 + \Sigma(\omega) \tag{2}$$

consists of the energy of the bare transverse exciton and its self-energy. The observed transverse exciton energy ω_T satisfies

$$\omega_T = \omega_1 + \Sigma(\omega_T). \tag{3}$$

If we set $\omega_1 = \omega_T$ in Eq. (2) and ignore the rest of the level shift, then $\Sigma(\omega)$ becomes purely absorptive and may be written $\Sigma(\omega) = -i\frac{1}{2}\gamma(\omega)$. Structure in the function $\gamma(\omega)$ will be caused by density-of-state effects (e.g., thresholds, Franck–Condon factors, etc.) described above. We have calculated $\gamma(\omega)$ from $\epsilon_1(\omega)$ and $\epsilon_2(\omega)$ and find the peaks to coincide with similar structures in $\epsilon_2(\omega)$ within ± 50 cm^{-1}. Therefore, we need focus attention only on the structure in $\epsilon_2(\omega)$ and $R(\omega)$ and leave differences between the $\epsilon_2(\omega)$ and $\gamma(\omega)$ spectra for a more accurate measurement of the optical constants.

The model represented by Eqs. (1) and (2) ignores spatial dispersion, i.e., the κ dependence of the dielectric function. The presence of spatial dispersion alters the picture in an essential way. Curvature in the ex-

citon band for κ perpendicular to the crystal face will result in reduced reflectivity for the single-particle region.[17] However, in crystals of neutral organic molecules there is no evidence of electron exchange interactions between neighbors of magnitude sufficient to create large spatial dispersion in the region of optical wavevectors. Dipole interactions will undoubtedly give rise to some dispersion, especially for (010) planes which are only 3.53 Å apart, however, this dispersion will only be evident at wave vectors $\kappa \gg q_{\text{photon}}$. Therefore, spatial dispersion will be excluded from further consideration.

After discussing the dressed polariton picture and its relation to the overall shape of the reflection spectrum, we turn now to a more detailed discussion of the structure observed at the low energy side. The reflectivity between 450 and 425 nm was observed to increase greatly upon cooling from 300 to 5 K. This effect is due to the freezing out of lattice phonons and some low frequency intramolecular modes. In the region of the lowest energy peak at 444 nm (see Fig. 1) there is no sign of a lattice phonon. In the low temperature Raman spectrum there are six librational modes between 40 and 180 cm^{-1}. The upper end of this range overlaps the lowest frequency intramolecular mode so that there is no clean separation between inter- and intramolecular modes. The absence of phonon structure implies that exciton–lattice phonon coupling is weak, a view consistent with the concept that a strong molecular transition gives rise to an excitation that propagates so rapidly that the lattice has no time to react to its passage. We also note that in Fig. 2 there is a considerable concentration of intensity in the "zero-phonon" transition at ω_T, which has the characteristic spike shape expected in the strong coupling regime.

The main structure in the ϵ_2 spectrum measured relative to $\omega_T = 22\,420$ cm^{-1} (± 25 cm^{-1}) occurs at 200 (sh), 450 (max), 600 (sh), 1350 (sh), 1600 (sh), 1750 (max), and 2400 (max). Here sh means shoulder, max means maximum, and all energies are in cm^{-1}. The error is considerable, at least ± 50 cm^{-1} for the maxima, and higher still for the shoulders. The prominent totally symmetric Raman modes of $TCNQ^0$ are 144, 334, 602, 711, 943, 1207, 1454, 1602, 2229, and 3048 cm^{-1}.[18] All the peaks and shoulders can be assigned as either fundamental or combinations of these a_{1g} modes within the accuracy of the derived ϵ_2 spectra. They are interpreted as being due to multiparticle edges or peaks in the density of states.

The structure between 445 and 430 nm seems subject to the least ambiguity. The reflectivity starts to decrease sharply at $\omega_T + 150$ cm^{-1}, with a shoulder around $\omega_T + 250$ cm^{-1}. A second sharp decrease occurs at $\omega_T + 350$ cm^{-1}, followed by a distinct minimum at $\omega_T + 470$ cm^{-1}. We tentatively assign the sharp decreases as due to thresholds for the 144 and 334 cm^{-1} intramolecular vibrations, and the minimum at $\omega_T + 470$ cm^{-1} (which transforms into a ϵ_2 peak at $\omega_T + 450$ cm^{-1}) to a combination of the 144 and 334 cm^{-1} vibrations. The latter structure may be due to a maximum in the combined density of states or a two phonon threshold. This interpretation is wholly consistent with strong coupling theory; however, it does not constitute proof of the validity of the theory since the structure in the spectra is not sharp enough for the assignments given above to be considered definite. It was mentioned earlier that the conglomeration of transitions between 24 000 and 25 000 cm^{-1} is responsible for the main minimum in the reflection spectra at 422 nm. The foregoing analysis would assign all these transitions to fundamentals and combinations. However, this neglects the possibility of single-particle resonances buried in the band. In the single-particle picture (no intensity carried by the multiparticle states) these transitions correspond to the higher vibronic transitions in the isolated molecule in which C–C stretching modes are excited. They will be clustered more towards the center of gravity of the exciton band, and will enhance the intensity of nearby two-particle transitions.

IV. CONCLUSION

Crystalline $TCNQ^0$ is the first "metallic reflector" shown to have vibrational fine structure in its low temperature spectrum. Kramers-Kronig transformation has revealed that there are large regions where $\epsilon_1 < -1$, implying that surface polaritons should be observable. In agreement with the basic ideas of strong vibronic coupling theory there is no lattice phonon structure, implying that the exciton propagates without lattice relaxation. Structure in the low energy side of the reflection band is also consistent with the concepts of strong coupling theory. However, a detailed vibrational analysis of the $TCNQ^0$ reflection spectrum using simplified ideas of strong coupling theory cannot be made in a convincing manner. What is needed now is a theory of strong vibronic coupling detailed enough to allow the inclusion of all a_{1g} modes that large molecules possess, and powerful enough to permit the calculation of highly anisotropic optical properties of organic crystals.

[1] L. B. Clark, J. Chem. Phys. **51**, 5719 (1969).
[2] L. B. Clark and M. R. Philpott, J. Chem. Phys. **53**, 3790 (1970).
[3] L. B. Clark and L. Hymowitz (private communication).
[4] E. E. Koch and A. Otto, Phys. Status Solidi B **51**, 69 (1972).
[5] E. E. Koch and A. Otto, Chem. Phys. **3**, 370 (1974).
[6] R. R. Pennelly and C. J. Eckhardt, Chem. Phys. **12**, 89 (1976).
[7] B. G. Annex and W. T. Simpson, Rev. Mod. Phys. **32**, 466 (1960).
[8] B. M. Fanconi, G. A. Gerhold, and W. T. Simpson, Mol. Cryst. Liq. Cryst. **6**, 41 (1969).
[9] R. E. Long, R. A. Sparks, and K. N. Trueblood, Acta. Crystallogr. **18**, 932 (1962).
[10] H. J. Hesse, W. Fuhs, G. Weiser, and L. Von Szentpaly, Chem. Phys. Lett. **41**, 104 (1976); Phys. Status Solidi (B) **76**, 817 (1976).
[11] W. T. Simpson and D. L. Peterson, J. Chem. Phys. **26**, 588 (1957).
[12] M. R. Philpott, J. Chem. Phys. **52**, 5842 (1970); **54**, 2120 (1971).

[13]The stop band is the region between the upper and lower branches of a simple polariton in a crystal with no damping and no spatial dispersion.
[14]M. R. Philpott and J-M. Turlet, J. Chem. Phys. **64**, 3852 (1976).
[15]M. R. Philpott, J. Chem. Phys. **55**, 2039 (1971).
[16]P. B. Johnson and R. W. Christy, Phys. Rev. **6**, 4370 (1972).
[17]J. J. Hopfield and D. G. Thomas, Phys. Rev. **132**, 563 (1963).
[18]A. Girlando and C. Pecile, Spectrochim. Acta Part A **29**, 1859 (1973).